

## ■ Supplementary Information

### **Highly Efficient Plastic Crystal Ionic Conductors for Solid-state Dye-sensitized Solar Cells**

*Daesub Hwang<sup>ab</sup>, Dong Young Kim<sup>b</sup>, Seong Mu Jo<sup>b</sup>, Vanessa Armel<sup>c</sup>, Douglas R. MacFarlane<sup>c</sup>, Dongho Kim<sup>a\*</sup>, and Sung-Yeon Jang<sup>d\*</sup>*

<sup>a</sup>*Department of Chemistry, Yonsei University, Seoul 120-749, Korea*

<sup>b</sup>*Optoelectronic Materials Lab, Korea Institute of Science and Technology, Seoul 136-791, Korea*

<sup>c</sup>*Australian Centre for Electromaterials Science, School of Chemistry, Monash University, Clayton, VIC 3800, Australia*

<sup>d</sup>*Department of Chemistry, Kookmin University, Seoul 136-702, Korea*

**Correspondance to** [dongho@yonsei.ac.kr] and [syjang@koomin.ac.kr]

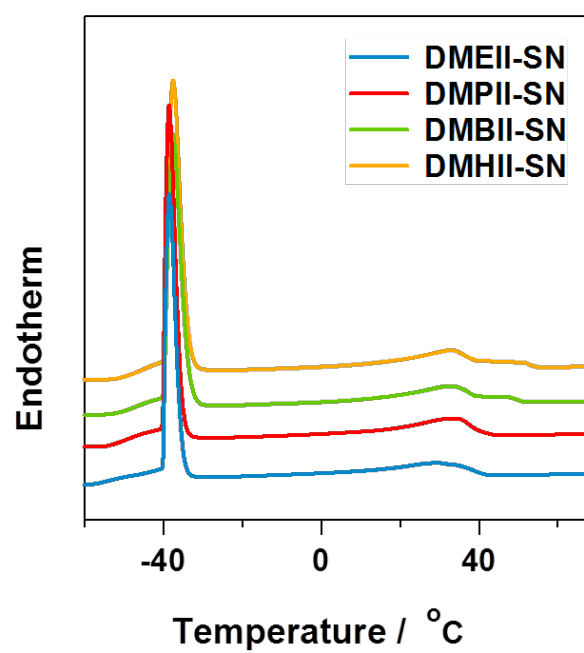


**Fig. S1** Differential scanning calorimetric thermograms of plastic crystal electrolytes doped with four different ionic conductors (concentration: 6 mol. % for DMAII, respectively)

**Table S1** Details of the thermal energies of transition for plastic crystal electrolytes calculated from differential scanning calorimetric thermograms (as shown in figure S1).

Electrolyte	Enthalpy Change	
	Solid State at -39 °C ( $\Delta H, \text{Jg}^{-1}$ )	Plastic Phase at 35 °C ( $\Delta H, \text{Jg}^{-1}$ )
DMEII-SN	45.3	12.8
DMPII-SN	60.6	14.4
DMBII-SN	63.3	19.3
DMHII-SN	65.4	22.2

## Electrospray Methods & Hierarchically structured TiO<sub>2</sub> beads

The electrostatic spray (e-spray) technique has recently been used as a cheap and simple process to directly deposit thin films from their colloidal solutions. During e-spray deposition, the solutions become mechanically atomized into droplets, and the surface of droplets is charged because of the electric field. The electric field develops an electric charge on the liquid surface. Also, the charge remains on the droplets as they detach from the jet. The magnitude of the charge on a droplet is given by the equation,  $Q_R = 2\pi(16\sigma_1\epsilon_0r^3)^{1/2}$ , where  $\sigma_1$  is the liquid surface tension,  $\epsilon_0$  is the dielectric permittivity of the free space, and  $r$  is the droplet radius. The deposition efficiency of the charged droplets is usually much higher than that of uncharged droplets, so the adhesion between the materials and substrates is often improved. The e-spray process is generally performed at room temperature under atmospheric pressure, which significantly reduces equipment costs.

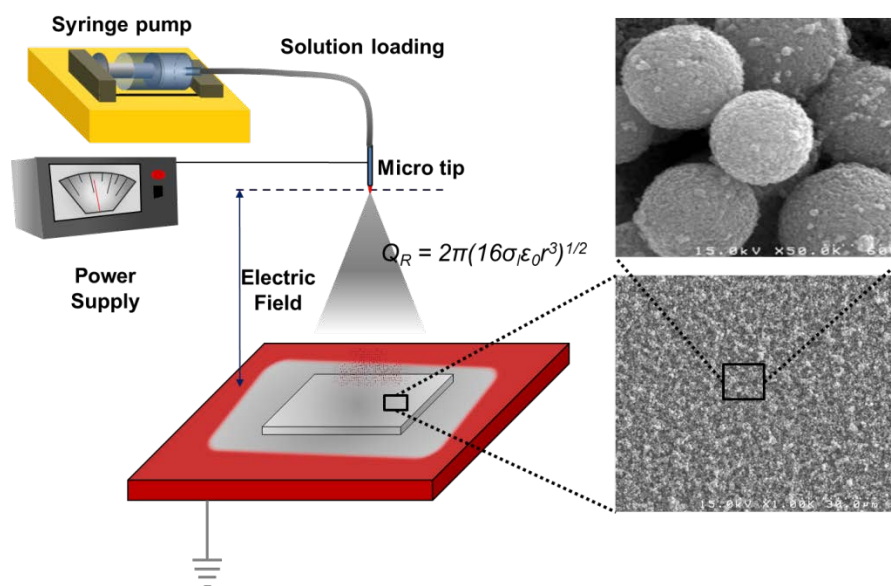


**Fig. S2** Electrostatic spray process to prepare the photoelectrodes composed of hierarchically-structured TiO<sub>2</sub> spheres (TiO<sub>2</sub>-SP).

## Electrochemical impedance spectroscopy (EIS) analysis

Electrochemical impedance spectroscopy (EIS) analysis was performed following the models of Adachi et al.<sup>[1]</sup>, who showed the equivalence of models developed by Kern et al.<sup>[2]</sup> and Bisquert.<sup>[3]</sup> The AC impedance measurements provide information on the fundamental properties of the cells, including the material quality and interfacial phenomena, and can be used to understand the origin of the improved FF and PCE in our DSSCs. The complex impedance of a typical DSSC is the sum of each of the components, given as  $Z_0$ ,  $Z_1$ ,  $Z_2$ , and  $Z_3$ . The components are defined as the contact impedance,  $Z_0$ , which is usually equal to the real-phase component  $R_S$ ; the counter electrode impedance,  $Z_1$ ; the complex impedance,  $Z_2$ , which represents the interfaces amongst the dye-attached semiconductors and between the semiconductors and electrolyte; the diffusion of triiodide ion-related (Warburg) impedance,  $Z_3$ . Thus, total  $Z$  ( $Z' + iZ''$ ) is equal to the sum  $Z_0 + Z_1 + Z_2 + Z_3$ , as shown in Fig. S2A. An idealized plot of the real part of  $Z$ ,  $Z'(\omega)$ , versus the imaginary part of  $Z$ ,  $Z''(\omega)$ , over a wide frequency range for a particular set of conditions is given in Fig. S2B. In general, three semicircles are clearly observed clearly in the measured frequency range 0.1–100 kHz. The internal series resistance ( $R_S$ ) in the high-frequency region conforms to the electrolyte/FTO glass resistance, whereas the resistances  $R_{Pt}$ ,  $R_{CT}$ , and  $R_D$  relate to the charge-transfer resistance of the electrolyte at the counter electrode surface in the higher-frequency region ( $R_{Pt}$ ), the resistance reflecting the photoinjected electrons within the  $TiO_2$  in the intermediate-frequency region ( $R_{CT}$ ), and the resistance corresponding to the Nernst diffusion within the electrolyte in the low-frequency region ( $R_D$ ).

- [1] M. Adachi, M. Sakamoto, J. Jiu, Y. Ogata and S. Isoda, *J. Phys. Chem. B*, **2006**, 110, 13872.
- [2] R. Kern, R. Sastrawan, J. Ferber, R. Stangl and J. Luther, *Electrochim. Acta*, **2002**, 47, 4213.
- [3] J. Bisquert, *J. Phys. Chem. B*, **2001**, 106, 325.

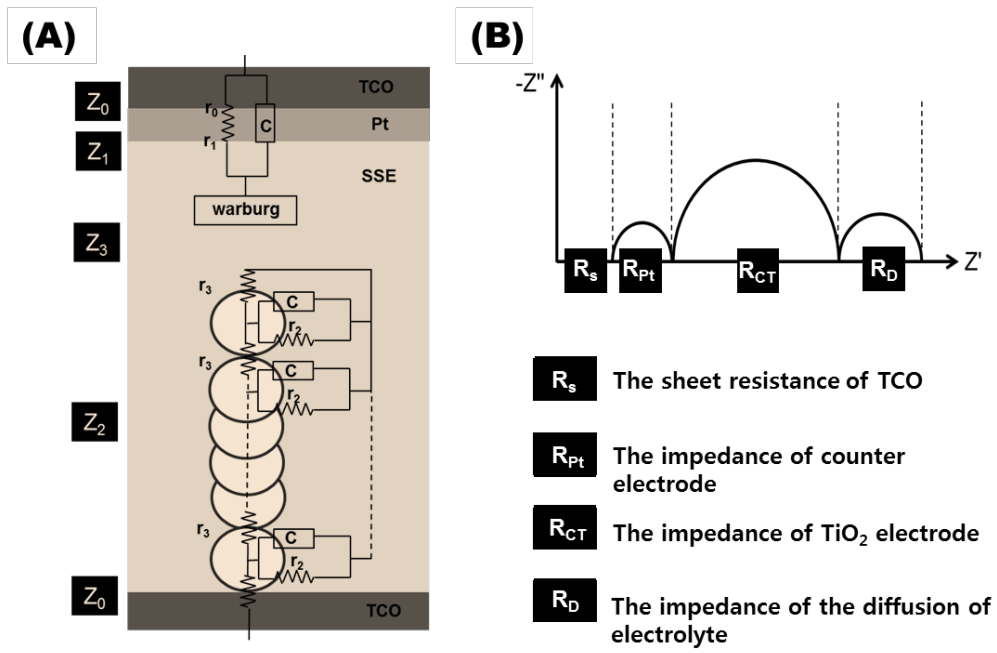


**Fig. S3** (A) Equivalent electrical circuit representation for DSSCs. (B) Ideal impedance plane plot for a DSSC, showing the real parts of the impedances  $R_s$ ,  $R_{Pt}$ ,  $R_{CT}$ , and  $R_D$ .

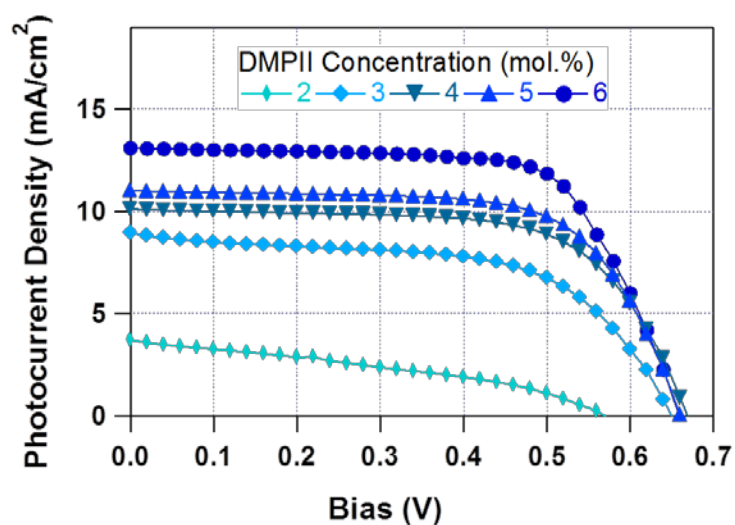


**Fig. S4** Photovoltaic properties of the J-V curves depending on DMPII concentrations (mol.%) measured under simulated AM 1.5G one sun light intensity.

**Table S2** Summary of Photovoltaic Properties of the DSSCs Using Diverse DMPII concentrations solid-state electrolyte.

DMPII Conc. (mol.%)	$V_{oc}$ (V)	$J_{sc}$ ( $\text{mA}/\text{cm}^2$ )	FF	EFF (%)
2	0.570	3.7	0.361	0.76%
3	0.650	8.9	0.584	3.39%
4	0.668	10.1	0.656	4.43%
5	0.660	11.0	0.671	4.88%
6	0.651	13.0	0.685	5.93%

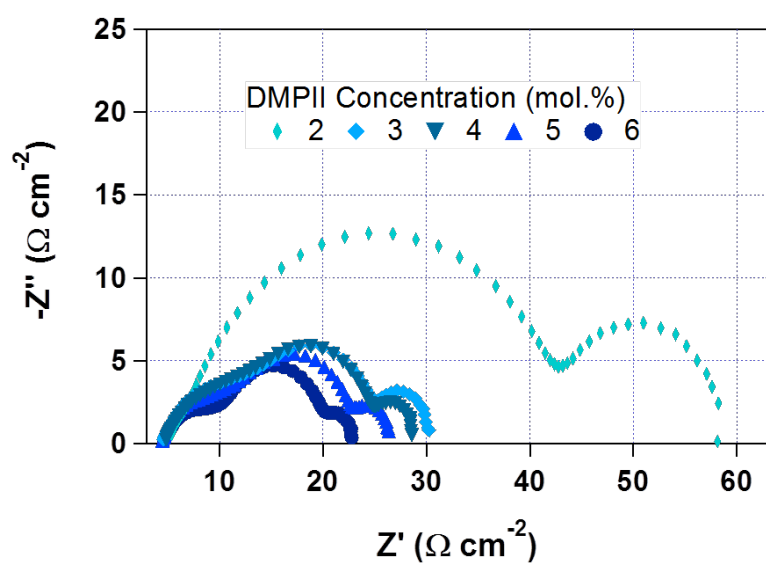


**Fig. S5** Electrochemical properties of the Nyquist plots depending on DMPII concentrations (mol.%) measured by EIS analyzer.



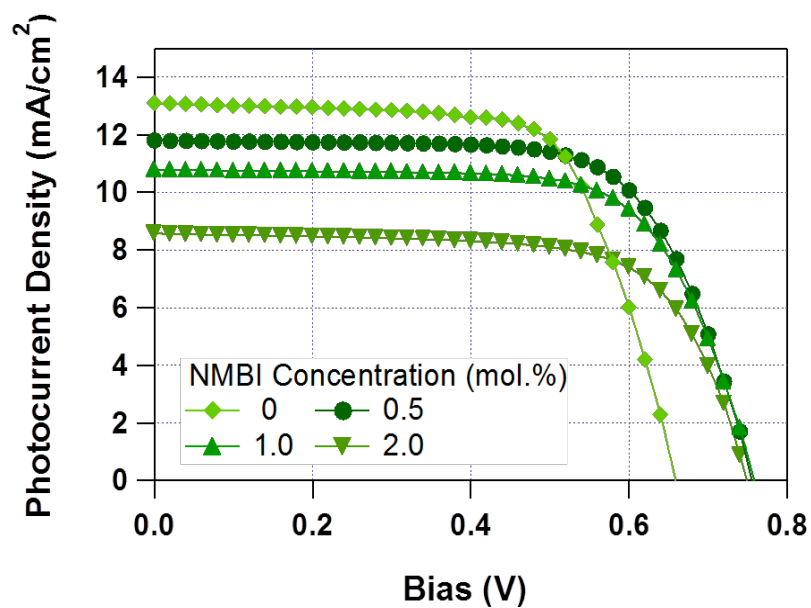


**Fig. S6** Photovoltaic properties of the J-V curves depending on NMBI concentrations (mol.%) measured under simulated AM 1.5G one sun light intensity.

**Table S3** Summary of photovoltaic properties of the DSSCs using diverse NMBI concentrations solid-state electrolyte.

NMBI Conc. (mol.%)	$V_{oc}$ (V)	$J_{sc}$ (mA/cm <sup>2</sup> )	FF	EFF (%)
0	0.66	13.1	0.68	5.81%
0.5	0.75	11.9	0.69	6.21%
1	0.76	10.8	0.69	5.68%
2	0.76	8.6	0.69	4.45%

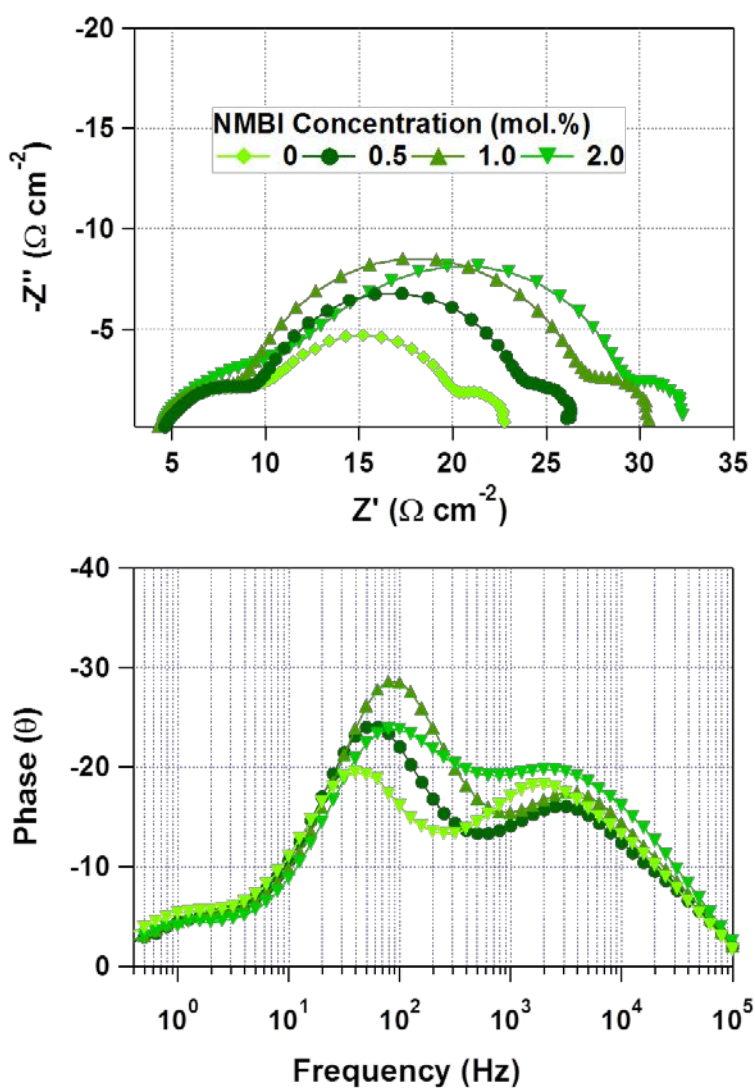


**Fig. S7** EIS analysis results of the diverse ss-DSSCs in open-circuit conditions under simulated AM 1.5 G illumination; Nyquist plot for the frequency range  $10^{-1}$  to  $10^5$  Hz; corresponding Bode phase plots.

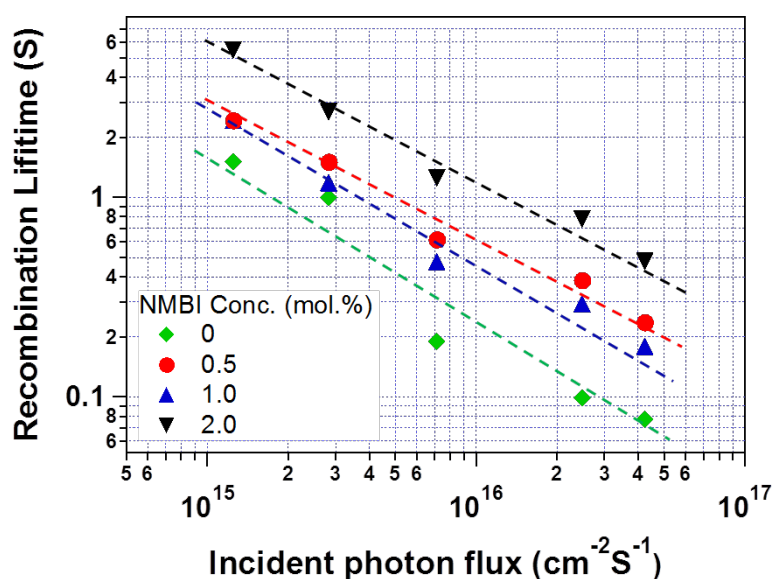


**Fig. S8** Intensity-modulated photovoltage spectroscopy (IMVS) plots of the ss-DSSCs depending on NMBI concentrations (mol.%). The electron-recombination lifetimes were measured intensity-modulated photovoltage spectroscopy (IMVS). A diode laser with variable power and modulation control (Coherent CUBE diode-laser, 40 mW, 445 nm) was used as the light source for these studies. The illumination light was always incident on the working electrode side of the solar cells. The intensity was measured using a calibrated Si photodiode. The output of the solar cell was connected directly to a lock-in amplifier (Frequency Response Analyzers, Solatron 1260 Impedance/ Gain-Phase Analyzer). During the IMVS measurements, the cell was illuminated with sinusoidally modulated light having a small AC component (10% or less of the DC component).

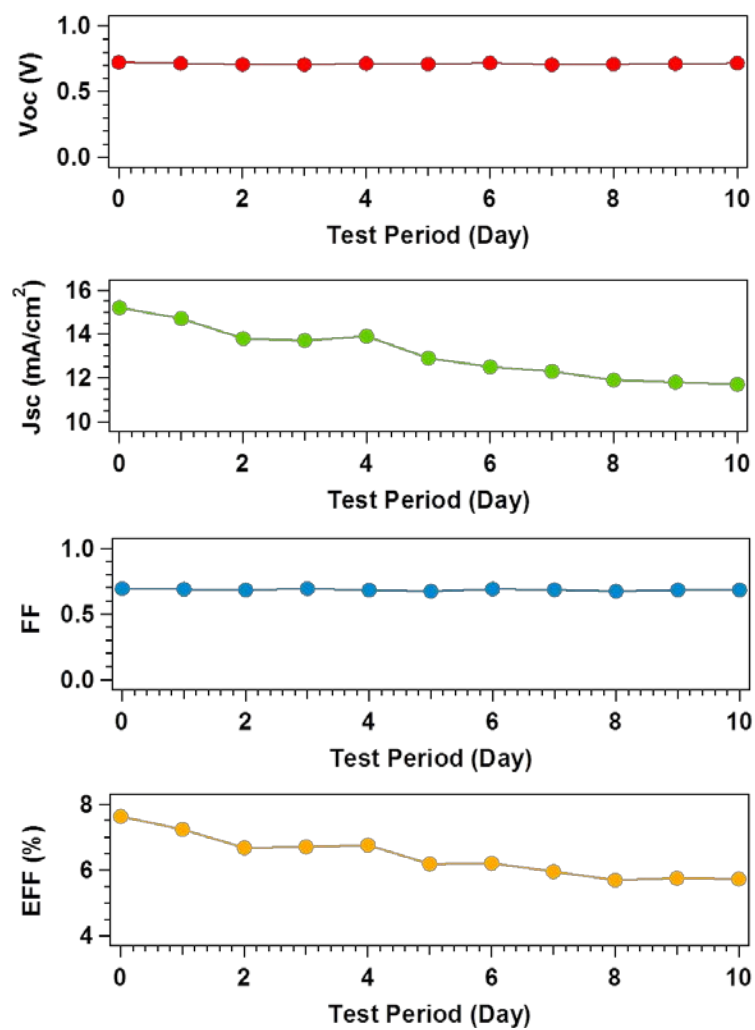


**Fig. S9** The results for the stability test of solid-state DSSCs using DMPII-SN.